Extraction of Chemical Reactivity and Structural Relaxations of an Organic Dye from the Short-Range Interaction with a Molecular Probe

Karl Rothe, Nicolas Néel, Marie-Laure Bocquet, Jörg Kröger

Extraction of Chemical Reactivity and Structural Relaxations of an Organic Dye from the Short-Range Interaction with a Molecular Probe

Karl Rothe,[†] Nicolas Néel,[†] Marie-Laure Bocquet,[‡] and Jörg Kröger[*,†]

†*Institut für Physik, Technische Universität Ilmenau, D-98693 Ilmenau, Germany*

‡*PASTEUR, Département de chimie, École normale supérieure, PSL University, Sorbonne Université, CNRS, F-75005 Paris, France*

E-mail: joerg.kroeger@tu-ilmenau.de

Abstract

A CO-functionalized atomic force microscope tip is used to locally probe local chemical reactivity and subtle structural relaxations of a single phthalocyanine molecule at different stages of pyrrolic-H abstraction. Spatially resolved vertical force spectroscopy unveils a variation of the maximum short-range attraction between CO and intramolecular sites, which is interpreted as a measure for the local chemical reactivity. In addition, the vertical position of the point of maximum attraction is observed to vary across the molecules. These changes follow calculated adsorption heights of the probed molecular atoms.

Graphical TOC Entry

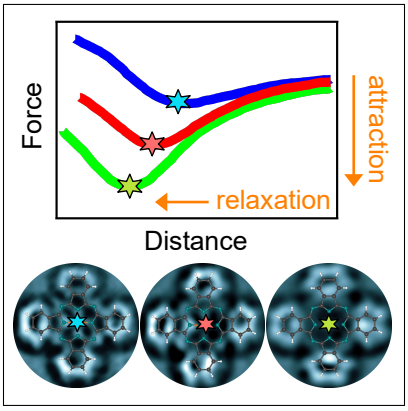

The invention of the atomic force microscope (AFM)[1] was motivated by the desire to image surfaces of insulators with similar spatial resolution as provided by the scanning tunneling microscope (STM)[2] for metal or semiconductor surfaces. Since then, the AFM has developed into a powerful method for exploring quantum chemistry and physics at surfaces. Besides the capability of manipulating matter at the atomic scale,[3,4] two experimental achievements were important for this stupendous evolution of the AFM, i. e., the use of a piezoelectric tuning fork as a force probe[5,6] and the termination of the tip apex with a single molecule for imaging with submolecular resolution.[7,8]

With these tools at hand the chemical bond order was determined[9] and intramolecular changes upon chemical reactions were identified.[10] The subpicometer control of the distance between an intentionally terminated AFM tip and the surface further enabled the observation of the interaction between reaction partners at the single-atom and single-molecule level, such as the coupling between two CO molecules,[11] the bending of molecular adsorbates in the vicinity of a CO-terminated tip,[12] the probing of physisorbed and chemisorbed states in a CO–Fe contact,[13] relaxations[14] and nonequilibrium bond forces[15] in C_{60}–C_{60} junctions, the identification of chemically reactive Fe cluster sites,[16] the motion of atomic[17] and molecular[18] terminations of the tip apex in the vicinity of the surface as well as forces and energies at the verge of a chemical reaction.[19] Moreover, insights into the force fields atop adsorbed molecules,[20] the resolution of H atoms at the onset of Pauli repulsion between the functionalized probe and the imaged molecule[21] as well as the anisotropic charge distributions at surfaces[22] were reported.

In the work presented here, the magnitude and position of the maximum short-range attraction between a CO-terminated AFM tip and specific sites of a single phthalocyanine ($C_{32}H_{18}N_8$, 2H-Pc) molecule adsorbed on Ag(111) are used to extract information on local chemical reactivity and structural relaxations. The feasibility of this approach is demonstrated for the different stages of pyrrolic-H abstraction of a single phthalocyanine – 2H-Pc, H-Pc and Pc. In spatially resolved force spectroscopy across the molecule species the point

of maximum short-range attraction (PMA) gradually increases its magnitude and vertically shifts toward the surface upon laterally approaching the macrocycle center from the molecular periphery. The effect is most pronounced for Pc. While the progressive increase of the PMA magnitude toward the central molecular region is rationalized in terms of an enhancement of the local chemical reactivity, the PMA vertical shifts are in agreement with the variations of equilibrium atomic adsorption heights resulting from density functional simulations.

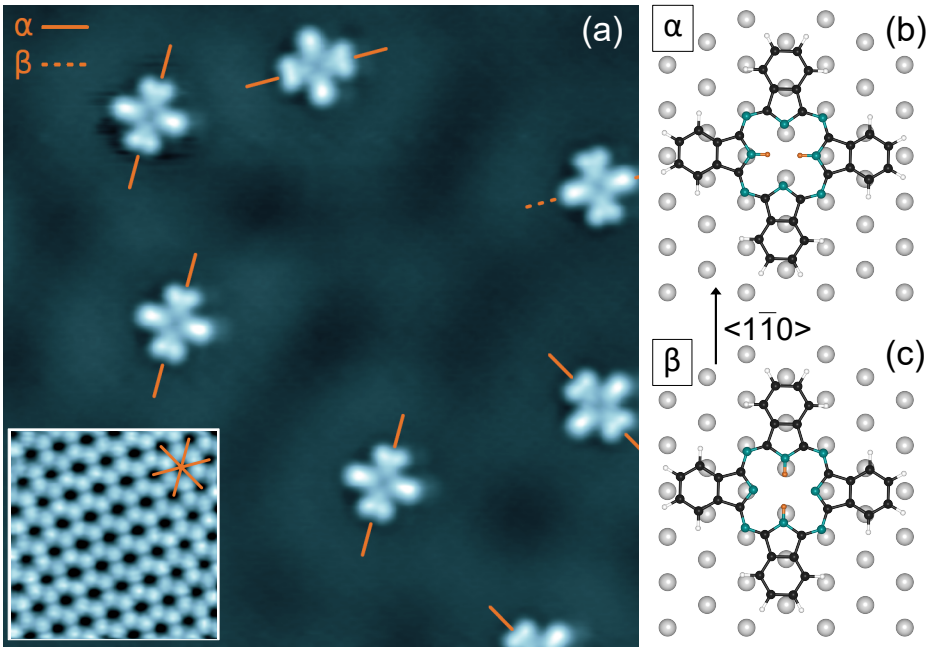

Figure 1: (a) STM data of Ag(111) and adsorbed 2H-Pc molecules acquired with a CO-terminated tip (bias voltage: 50 mV, tunneling current: 15 pA, size: 15 nm × 15 nm). Molecular species α and β are oriented along crystallographic $\langle 1\bar{1}0 \rangle$ directions marked by solid and dashed lines attached to the imaged molecules. Inset: Atomically resolved STM image of Ag(111) obtained by dragging a Ag atom across the surface (10 mV, 0.5 μA, 2 nm × 2 nm). The lattice atoms appear as circular depressions. Lines indicate $\langle 1\bar{1}0 \rangle$ directions. (b), (c) Possible adsorption geometries of α and β species of 2H-Pc.

Individual 2H-Pc molecules are well separated from each other at the low surface coverage used in the experiments (Figure 1a). In STM images, they exhibit a cloverlike shape with C_2 symmetry. One pair of opposite isoindole moieties appears higher than the other pair, which instead exhibits two lobes rather than one at the periphery. Two 2H-Pc orientations referred to as α (Figure 1b) and β (Figure 1c) are found on the surface. The orientation of

α (β) molecules is characterized by the pyrrolic H–H axis aligned perpendicular (parallel) to a crystallographic $\langle 1\bar{1}0 \rangle$ direction. The latter can be inferred from atomically resolved STM images of the surface (inset to the STM image in Figure 1a). In a previous report,[23] α and β species of 2H-Pc were reversibly interconverted through a tautomerization reaction, which was induced by abruptly raising the bias voltage above 0.45 V. In the present case, where bias voltages did not exceed 0.1 V and, thus, did not stimulate tautomerization, α and β molecules are present a priori after adsorption with a ratio of $\alpha : \beta \approx 6 : 1$. This observation is in agreement with calculations that assigned the α species of 2H-Pc on Ag(111) to an adsorption geometry that is preferred by ≈ 0.2 eV compared to the β species.[24] In the following, the presented studies focus on the most abundant α species.

The stepwise removal of pyrrolic H follows a previously reported protocol.[25] Figure 2a shows that the bias voltage has to be ramped to 3 V after positioning the tip atop the macrocycle center of intact 2H-Pc and deactivating the feedback loop. The consecutive abstraction of the first and second pyrrolic H is signaled by sharp decreases of the current (arrows). The locally injected electrons deposit their energy into the excitation of molecular vibrational quanta that involve the N–H bond,[26] which finally breaks, releases the H atom and leaves behind an unsaturated N· bond. The latter is quickly saturated by hybridization with the Ag(111) surface.

To see potential structural changes clearly, AFM images of all molecules – 2H-Pc, H-Pc, Pc – were acquired with a CO-terminated tip in the Pauli repulsion range of distances (Figure 2b–d). For each constant-height map of the resonance frequency change Δf, a ball-and-stick model of the molecule is superimposed. Bright contrast in the Δf maps is therefore due to the C–C and C–N bonds of the isoindole moieties. The C–H bonds at the periphery of the molecule also leave their fingerprint in the spatially resolved Δf data, which is in agreement with previous reports on other molecules.[7,27,28] The center of the macrocycle of 2H-Pc (Figure 2b) exhibits two bright elongated protrusions, which are associated with the intact pyrrolic N–H bonds. This assignment is based on the comparison of AFM and STM images. In

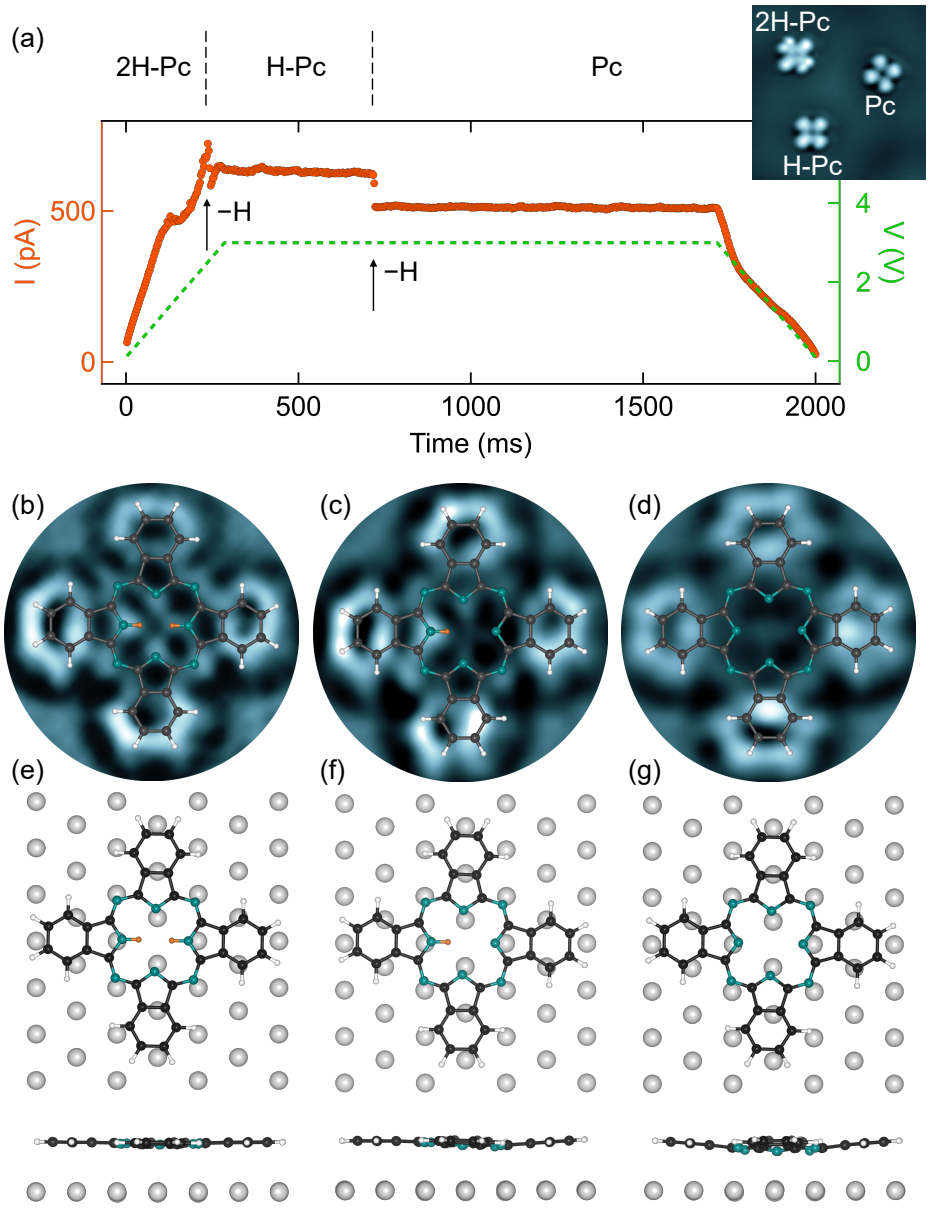

Figure 2: (a) Tunneling current I and bias voltage V used for the single-molecule reaction 2H-Pc$\xrightarrow{-\mathrm{H}}$H-Pc$\xrightarrow{-\mathrm{H}}$Pc. Inset: STM image of 2H-Pc, H-Pc and Pc after successful reactions (50 mV, 15 pA, 8 nm × 8 nm). (b)–(d) AFM images of (b) 2H-Pc, (c) H-Pc and (d) Pc acquired with a CO-terminated tip at 10 mV and at a Pauli repulsion distance. The gray scales from black to white encode resonance frequency changes from (b) −10 to 3 Hz, (c) −12 to −2 Hz and (d) −10 to 2 Hz. (e)–(g) Calculated relaxed adsorption geometries for (e) 2H-Pc, (f) H-Pc and (g) Pc viewed from the top (top row) and the side along a ⟨010⟩ direction (bottom).

the latter, isoindole groups with N–H bonds are characterized by brighter contrast.[23–25,29] Expectedly, for H-Pc (Figure 2c) only one N–H bond is visible, while they are entirely missing for Pc (Figure 2d). Although the model structures are to scale with the AFM data, deviations are clearly visible. They are assigned to the propensity of the CO probe to bend at the AFM tip when it is subject to strong forces at chemical-bond distances.[11,18,30] This CO flexibility leads to the apparent distortion of the molecular structure. The Supporting Information present AFM images of the molecules at different tip–molecule separations.

The overall reduction of the contrast in the macrocycle center in the course of pyrrolic-H abstraction is not only due to the successively missing N–H bonds. The calculated adsorption geometries of the molecules on Ag(111) (Figure 2e–g) reveal that the planar geometry of intact 2H-Pc (Figure 2e) progressively transforms into an inverted dome shape for H-Pc (Figure 2f) and Pc (Figure 2g). The removal of pyrrolic H leaves behind a dangling N· bond that binds to the metal surface and concomitantly distorts the molecular plane. Similar deformations upon dehydrogenation were reported for Sn-Pc on Ag(111),[31] pentacene on Ag(110)[32] and asphaltenes on Cu(111);[33] the bending of the molecular plane du to N–metal bonds was likewise observed for *meso*-dibenzoporphycene on Ag(111).[34]

Figure 3 presents the main experimental results of this work. The high spatial resolution offered by the CO-terminated tip was used for the pointwise probing of the vertical short-range force $F(z)$ (z: tip displacement along the surface normal with approach direction from positive to negative z, arrow in Figure 3b) atop various molecular sites along the isoindole moieties, between the periphery and the center of the macrocycle. The short-range component of the total vertical force is obtained by comparing resonance frequency changes Δf_0 on clean Ag(111) with Δf measurements atop all molecules at the same initial tip–surface distance and with the same CO-terminated tip.[15,19,35–37] To this end, the apparent heights of the different molecule species with respect to the Ag(111) surface are determined using identical feedback loop parameters that are set prior to resonance frequency spectroscopy (Supporting Information). In the thus rescaled tip displacement z-axis (Figure 3), $z = 0$

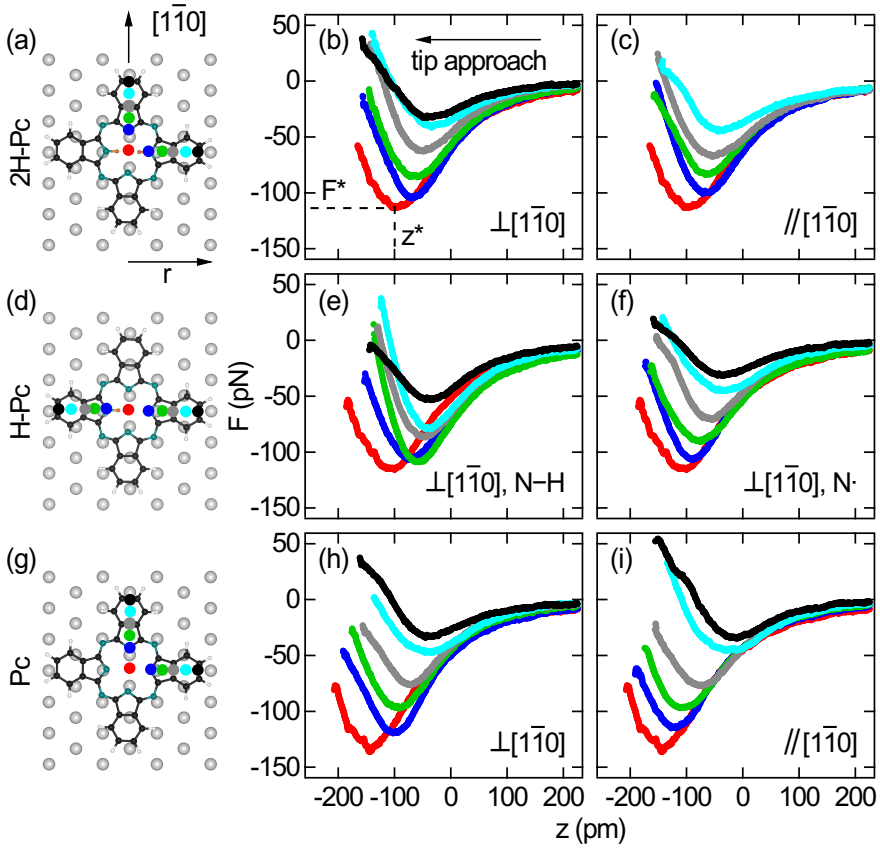

Figure 3: Spatially resolved short-range force $F(z)$ (see text) acquired on (a)–(c) 2H-Pc, (d)–(f) H-Pc, (g)–(i) Pc with a CO-terminated tip at 10 mV. For 2H-Pc and Pc, isoindole groups are probed perpendicular ($\perp$) and parallel ($\parallel$) to $\langle 1\bar{1}0\rangle$, while for H-Pc the $\perp$ direction comprising both the intact (N–H) and the H-abstracted (N·) isoindole moieties is investigated. In all $F(z)$ traces, $z = 0$ defines the tip displacement at which the feedback loop was deactivated above the clean Ag(111) surface (50 mV, 15 pA).

marks the tip–Ag(111) distance at the chosen feedback loop parameters. The difference $\Delta f(z) - \Delta f_0(z)$ with common z is then converted into $F(z)$ using previously reported algorithms.[38,39] Obviously, the PMA, which is defined by the minimum $F^* = F(z^*)$ (Figure 3b), exhibits variations of its magnitude and position upon moving the CO probe across the molecule. A rationale for these two effects will be discussed next.

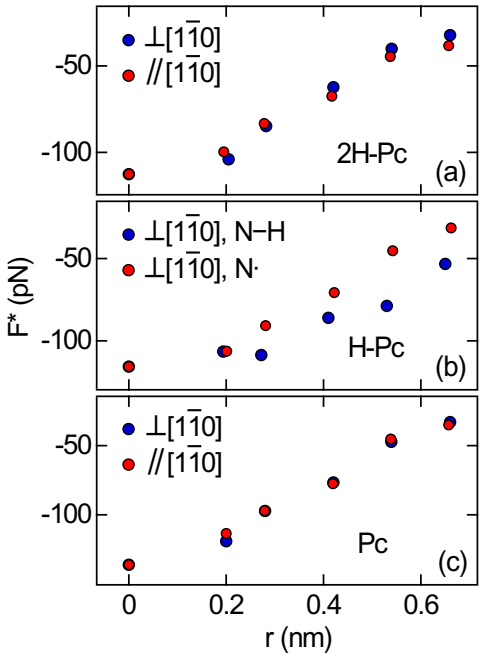

Figure 4: Spatially resolved short-range force $F^*(r)$ extracted from the $F(z)$ minima obtained on (a) 2H-Pc, (b) H-Pc, (c) Pc. Distances r are indicated in Figure 3a ($r = 0$: molecular center) and further defined in the Supporting Information.

The most important aspect conveyed by the $F(z)$ traces in Figure 3 is the evolution of the PMA magnitude, $F^*(r)$ (Figure 4). Because long-range contributions to the total vertical force were removed, F^* reflects the short-range attraction between the O atom of the CO-terminated tip and the approached intramolecular site. Therefore, the variations of F^* are interpreted in terms of spatial changes in the molecular chemical reactivity. A similar conclusion was drawn for the observed lateral alteration of F^* atop Fe clusters on Cu(111).[16] Indeed, the magnitudes of F^* are of the same order of magnitude in the present and previous[16] work. Before analyzing the data in more detail, the meaning of chemical

reactivity in the context of AFM measurements shall be specified. While chemical reactivity in general qualitatively characterizes the tendency of materials to form a chemical bond, F^* in short-range $F(z)$ traces indicates the strength of a bond. Therefore, it is reasonable to associate higher (lower) $|F^*|$, i. e., higher (lower) attraction at the PMA, with higher (lower) chemical reactivity.

For all molecules the most attractive site is the macrocycle center. The attractive force more than doubles from the 2H-Pc (Figure 4a) and H-Pc (Figure 4b) periphery to the center, and is nearly three times larger at the center of Pc (Figure 4c) than at its outer C–C benzene bond. In the case of Pc, the central attraction reaches its largest value, $\approx -136\,\mathrm{pN}$ in comparison with $\approx -116\,\mathrm{pN}$ (H-Pc) and $\approx -113\,\mathrm{pN}$ (2H-Pc). In a distance range excluding the molecular center, F^* varies in an almost linear manner. For 2H-Pc, the magnitude of F^* increases with similar slopes of $\approx 160\,\mathrm{pN/nm}$ and $\approx 136\,\mathrm{pN/nm}$ along isoindoline moieties oriented perpendicular and parallel to $\langle 1\bar{1}0\rangle$, respectively. Increased slopes of $\approx 188\,\mathrm{pN/nm}$ ($\perp$) and $\approx 178\,\mathrm{pN/nm}$ ($\parallel$) are observed for Pc, which are similarly comparable as in the case of 2H-Pc. However, clearly different slopes occur for H-Pc, i. e., $\approx 118\,\mathrm{pN/nm}$ along the intact isoindoline group and $\approx 165\,\mathrm{pN/nm}$ along the one with abstracted pyrrolic H. The difference in the slope clearly reflects the higher attraction atop the N$\cdot$ site compared to the intact N–H bond. This result together with the observations for Pc are consistent with previously reported metalation reactions where the phthalocyanine center encapsulates a metal atom from the gas phase or from an adsorbed phase at the surface.[40–43] The spatial variation of the PMA magnitude across the molecule measured here is therefore shown to represent a valuable experimental tool to determine the different chemically reactive sites of a single molecule, as previously demonstrated for adsorbed metal clusters.[16] In STM junctions, changes in the atomic-scale chemical reactivity were inferred from variations of the contact formation of a metal tip with C atoms of a buckled graphene lattice on Ru(0001).[44]

The vertical relaxations of the molecular plane that are visible in maps of Δf (Figure 2b–d) can be accessed in more detail using the vertical shift of the PMA position z^*. For 2H-

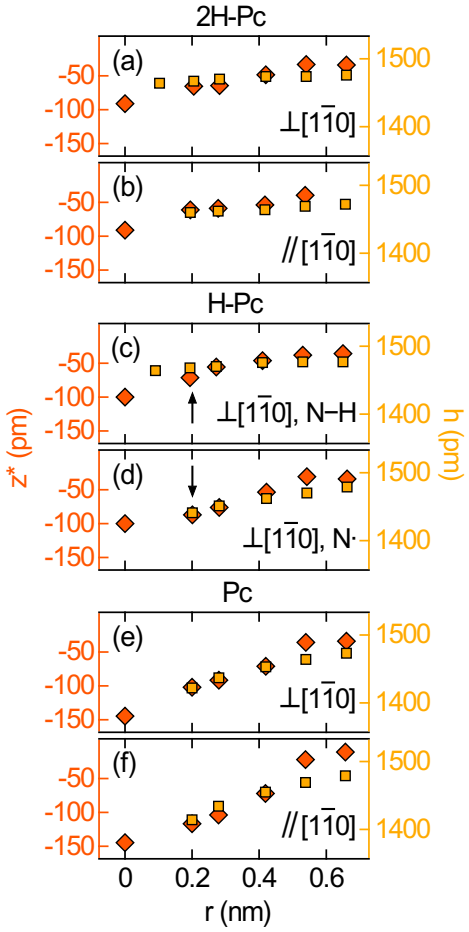

Figure 5: Force minima positions z^* (lozenges) for (a),(b) 2H-Pc, (c),(d) H-Pc and (e),(f) Pc as a function of the distance from the molecular center ($r = 0$) and in comparison with simulated adsorption heights h (squares). The scales for z^* as well as for h are identical for all plots ($-155\,\mathrm{pm} \leq z^* \leq -5\,\mathrm{pm}$, $1370\,\mathrm{pm} \leq h \leq 1520\,\mathrm{pm}$). Distances r are the same as in Figure 4.

Pc (Figure 5a,b) the isoindole groups oriented perpendicular and parallel to $\langle 1\bar{1}0\rangle$ exhibit a similar and weak variation of z^* (lozenges). In both cases, z^* tends to slightly decrease from the molecular periphery to the center. In order to compare the experimental findings with simulated data, the calculated adsorption heights h (squares in Figure 5a,b) of specific atoms of the molecule are used. For comparison with z^* determined above bonds rather than atop atoms, e. g., on top of a C–C bond, or above benzene and pyrrole centers, the arithmetic mean of h of, respectively, the two C atoms forming the bond or being closest to the centers were evaluated. These simulated data show the same trend as the experimental data, i. e., upon laterally approaching the macrocycle center h is reduced, which corresponds to the increased excursion of the tip to reach the PMA. Moreover, the variation of z^* and h in the molecular region excluding the center are comparably small, ≈ 31 pm (≈ 22 pm) for the $\perp$ ($\|$) direction in the experiments compared to 12 pm for both directions in the simulations. It reflects the virtually planar adsorption geometry of 2H-Pc. Quantitative deviations probably arise due to the tip–molecule proximity in the experiments, which distorts the simulated equilibrium adsorption geometry without tip.

The comparison of $z^*(r)$ and $h(r)$ in the case of 2H-Pc lends support to the idea that the spatially resolved probing of changes in the vertical position of the PMA reflects local variations of the adsorption height of the atomic constituents of the molecule. To further corroborate this idea, H-Pc (Figure 5c,d) and Pc (Figure 5e,f) were analyzed in the same manner. The isoindoline group of H-Pc comprising the intact N–H bond is similarly planar as observed for 2H-Pc, as judged from the small variation of z^* of ≈ 36 pm (Figure 5c); the opposite isoindole group with truncated N·, however, shows a discernible bending towards the Ag(111) surface, which is inferred from the increasing z^* by $\approx$ 53 pm observed upon laterally approaching N· from the benzene C–C bond at the periphery (Figure 5d). A similar difference in simulated adsorption heights is observed, 13 pm along the isoindoline moiety with intact N–H and 38 pm along the opposite isoindole group with N·. The arrows in Figure 5c,d mark the position of the intact N–H and dehydrogenated dangling N· bond

and reveal that the tip excursion z^* is higher by $\approx 16\,\mathrm{pm}$ in the case of N· (Figure 5d). This experimental observation is consistent with the simulated bending of the H-abstracted N· towards the surface in order to saturate the dangling N· bond. The lowering of the calculated N· adsorption height by 27 pm is in reasonable agreement with the increase of z^* from N–H to N·.

The deformation of the molecular plane close to the macrocycle center is most pronounced for Pc (Figure 5e,f). The strong shift of the PMA towards higher tip excursions in pointwise $F(z)$ traces reflects the inverted dome shape adopted by the molecule as a result of the two dangling N· bonds. Experimentally, z^* increases in a nearly linear manner by $\approx 68\,\mathrm{pm}$ ($\approx 106\,\mathrm{pm}$) perpendicular (parallel) to $\langle 1\bar{1}0\rangle$. Simulated adsorption heights (squares in Figure 5e,f) likewise exhibit an essentially linear behavior with a variation of the adsorption heights by 51 pm and 65 pm perpendicular and parallel to $\langle 1\bar{1}0\rangle$, respectively. Previously, shifts of the PMA were likewise interpreted as a manifestation of intramolecular adsorption heights[45] or as electric-field-induced relaxations of the junction.[14]

In conclusion, the spatial resolution of a CO-terminated AFM tip can be used to explore via pointwise spectroscopy of the short-range interaction the chemical reactivity of intramolecular moieties as well as their relaxed adsorption heights. The PMA *magnitude* is interpreted as a measure for the local reactivity, while its *position* reflects the variation of atomic adsorption heights. This approach has been applied to quantify the reactivity along the isoindoline moieties upon the atomwise abstraction of pyrrolic H as well as the transformation of the planar 2H-Pc adsorption geometry on Ag(111) to an inverted dome shape of Pc. The probing of local chemcial reactivity with a CO tip is therefore not restricted to localized d-electrons of inorganic transition-metal clusters; it is applicable to delocalized p-electrons of organic molecules, too.

Experimental method

A combined AFM and STM was operated in ultrahigh vacuum (10^{-9} Pa) and at low temperature (4.8 K). Surfaces of Ag(111) were cleaned by Ar^+ ion bombardment and annealing. Pure PtIr wire served as the tip material and was attached to the free prong of the piezoelectric tuning fork. Tips were repeatedly indented into the substrate surface and, thus, coated with a Ag film. The tip apex was further shaped by the transfer of single atoms from the tip to the surface.[46–50] Metal-free 2H-Pc molecules (purity: 98 %) were sublimated from a heated Ta crucible and deposited on clean Ag(111) at room temperature. CO molecules for tip termination were subsequently adsorbed on the cold (6 K) sample surface by backfilling the vacuum vessel with gaseous CO (purity: 99.97 %) at a partial pressure of 10^{-7} Pa and partially opened cryostat radiation shields. The transfer of a single CO molecule from the surface to the tip followed a standard routine.[51] For noncontact frequency modulation AFM data acquisition resonance frequency changes of the oscillating tuning fork (frequency: 29.9 kHz, amplitude: 30 pm, quality factor: 27000) were mapped at constant height. Resonance frequency changes as a function of the vertical separation to the surface were recorded after deactivating the feedback loop at 50 mV and 15 pA, followed by the retraction of the tip to the initial position and the ramping of the bias voltage to 10 mV. STM images were acquired in the constant-current mode with the bias voltage applied to the sample. AFM and STM data were further processed using WSxM.[52]

Theoretical method

Density functional calculations were carried out using the Vienna ab-initio simulation package[53] with the Perdew-Burke-Ernzerhof (PBE) exchange-correlation.[54] The projector-augmented wave potential with a standard cutoff energy of 400 eV was used to describe the electron–ion interaction.[55] Partial occupancies were determined by Gaussian scheme considering a low smearing of 0.05 eV. To account for van der Waals interactions and achieve

structural as well as electronic convergence the generalized-gradient-approximation PBE-D3 method[56] was used. The metallic surface was modeled by four atomic Ag layers and a rectangular $(7 \times 4\sqrt{3})$-Ag(111) unit cell embedded in about 1.4 nm of vacuum space. The used Ag lattice parameter of 0.4070 nm corresponds to a nearest-neighbor distance on Ag(111) of 0.2879 nm. The atomic positions of the topmost slab layer and the Ag-Pc molecule were relaxed until forces were smaller than 0.5 eV/nm at a single **k**-point (Γ) of the supercell Brillouin zone. These convergence criteria on the forces are sufficient for geometry determination.

Associated content

Supporting Information

The Supporting Information is available free of charge at https://pubs.acs.org/doi/...

Atomic force microscopy images at different vertical distances; definition of geometric distances; rescaling of the vertical-distance axis

Acknowledgement

Financial support by the Deutsche Forschungsgemeinschaft through Grant No. KR 2912/17-1 is acknowledged. The computational work was performed using the HPC ressources from GENCI-TGCC (Grant No. 2021 A9-A0070807364).

References

(1) Binnig, G.; Quate, C. F.; Gerber, C. Atomic Force Microscope. *Phys. Rev. Lett.* **1986**, *56*, 930–933.

(2) Binnig, G.; Rohrer, H.; Gerber, C.; Weibel, E. Surface Studies by Scanning Tunneling Microscopy. *Phys. Rev. Lett.* **1982**, *49*, 57–61.

(3) Becker, R. S.; Golovchenko, J. A.; Swartzentruber, B. S. Atomic-Scale Surface Modifications Using a Tunnelling Microscope. *Nature* **1987**, *325*, 419 – 421.

(4) Eigler, D. M.; Schweizer, E. K. Positioning Single Atoms with a Scanning Tunnelling Microscope. *Nature* **1990**, *344*, 524 – 526.

(5) Giessibl, F. J. High-Speed Force Sensor for Force Microscopy and Profilometry Utilizing a Quartz Tuning Fork. *Applied Physics Letters* **1998**, *73*, 3956–3958.

(6) Giessibl, F. J. The qPlus Sensor, a Powerful Core for the Atomic Force Microscope. *Review of Scientific Instruments* **2019**, *90*, 011101.

(7) Gross, L.; Mohn, F.; Moll, N.; Liljeroth, P.; Meyer, G. The Chemical Structure of a Molecule Resolved by Atomic Force Microscopy. *Science* **2009**, *325*, 1110–1114.

(8) Mönig, H.; Hermoso, D. R.; Díaz Arado, O.; Todorović, M.; Timmer, A.; Schüer, S.; Langewisch, G.; Pérez, R.; Fuchs, H. Submolecular Imaging by Noncontact Atomic Force Microscopy with an Oxygen Atom Rigidly Connected to a Metallic Probe. *ACS Nano* **2016**, *10*, 1201–1209.

(9) Gross, L.; Mohn, F.; Moll, N.; Schuler, B.; Criado, A.; Guitián, E.; Peña, D.; Gourdon, A.; Meyer, G. Bond-Order Discrimination by Atomic Force Microscopy. *Science* **2012**, *337*, 1326–1329.

(10) de Oteyza, D. G.; Gorman, P.; Chen, Y.-C.; Wickenburg, S.; Riss, A.; Mowbray, D. J.; Etkin, G.; Pedramrazi, Z.; Tsai, H.-Z.; Rubio, A. et al. Direct Imaging of Covalent Bond Structure in Single-Molecule Chemical Reactions. *Science* **2013**, *340*, 1434–1437.

(11) Sun, Z.; Boneschanscher, M. P.; Swart, I.; Vanmaekelbergh, D.; Liljeroth, P. Quantitative Atomic Force Microscopy with Carbon Monoxide Terminated Tips. *Phys. Rev. Lett.* **2011**, *106*, 046104.

(12) Hauptmann, N.; Groß, L.; Buchmann, K.; Scheil, K.; Schütt, C.; Otte, F. L.; Herges, R.; Herrmann, C.; Berndt, R. High-Conductance Surface-Anchoring of a Mechanically Flexible Platform-Based Porphyrin Complex. *New Journal of Physics* **2015**, *17*, 013012.

(13) Huber, F.; Berwanger, J.; Polesya, S.; Mankovsky, S.; Ebert, H.; Giessibl, F. J. Chemical Bond Formation Showing a Transition from Physisorption to Chemisorption. *Science* **2019**, *366*, 235–238.

(14) Brand, J.; Néel, N.; Kröger, J. Probing Relaxations of Atomic-Scale Junctions in the Pauli Repulsion Range. *New Journal of Physics* **2019**, *21*, 103041.

(15) Brand, J.; Leitherer, S.; Papior, N. R.; Néel, N.; Lei, Y.; Brandbyge, M.; Kröger, J. Nonequilibrium Bond Forces in Single-Molecule Junctions. *Nano Letters* **2019**, *19*, 7845–7851.

(16) Berwanger, J.; Polesya, S.; Mankovsky, S.; Ebert, H.; Giessibl, F. J. Atomically Resolved Chemical Reactivity of Small Fe Clusters. *Phys. Rev. Lett.* **2020**, *124*, 096001.

(17) Scheil, K.; Gruber, M.; Ondrácek, M.; Berndt, R. Force Spectroscopy of Iron Tetraphenylporphyrin Molecules with Cl Tips. *The Journal of Physical Chemistry C* **2020**, *124*, 26889–26896.

(18) Néel, N.; Kröger, J. Atomic Force Extrema Induced by the Bending of a CO-Functionalized Probe. *Nano Letters* **2021**, *21*, 2318–2323.

(19) Rothe, K.; Néel, N.; Bocquet, M.-L.; Kröger, J. Quantifying Force and Energy in Single-Molecule Metalation. *Journal of the American Chemical Society* **2022**, *144*, 7054–7057.

(20) Sweetman, A. M.; Jarvis, S. P.; Sang, H.; Lekkas, I.; Rahe, P.; Wang, Y.; Wang, J.; Champness, N.; Kantorovich, L.; Moriarty, P. Mapping the Force Field of a Hydrogen-Bonded Assembly. *Nature Communications* **2014**, *5*, 3931.

(21) Kawai, S.; Nishiuchi, T.; Kodama, T.; Spijker, P.; Pawlak, R.; Meier, T.; Tracey, J.; Kubo, T.; Meyer, E.; Foster, A. S. Direct Quantitative Measurement of the C=O$\cdots$H–C Bond by Atomic Force Microscopy. *Science Advances* **2017**, *3*, e1603258.

(22) Mallada, B.; Gallardo, A.; Lamanec, M.; de la Torre, B.; Špirko, V.; Hobza, P.; Jelinek, P. Real-Space Imaging of Anisotropic Charge of σ-Hole by Means of Kelvin Probe Force Microscopy. *Science* **2021**, *374*, 863–867.

(23) Kügel, J.; Sixta, A.; Böhme, M.; Krönlein, A.; Bode, M. Breaking Degeneracy of Tautomerization—Metastability from Days to Seconds. *ACS Nano* **2016**, *10*, 11058–11065.

(24) Granet, J.; Sicot, M.; Gerber, I. C.; Kremer, G.; Pierron, T.; Kierren, B.; Moreau, L.; Fagot-Revurat, Y.; Lamare, S.; Chérioux, F. et al. Adsorption-Induced Kondo Effect in Metal-Free Phthalocyanine on Ag(111). *The Journal of Physical Chemistry C* **2020**, *124*, 10441–10452.

(25) Sperl, A.; Kröger, J.; Berndt, R. Controlled Metalation of a Single Adsorbed Phthalocyanine. *Angewandte Chemie International Edition* **2011**, *50*, 5294–5297.

(26) Pecchia, A.; Romano, G.; Di Carlo, A. Theory of Heat Dissipation in Molecular Electronics. *Phys. Rev. B* **2007**, *75*, 035401.

(27) Zhang, J.; Chen, P.; Yuan, B.; Ji, W.; Cheng, Z.; Qiu, X. Real-Space Identification of Intermolecular Bonding with Atomic Force Microscopy. *Science* **2013**, *342*, 611–614.

(28) Jelínek, P. High Resolution SPM Imaging of Organic Molecules with Functionalized Tips. *Journal of Physics: Condensed Matter* **2017**, *29*, 343002.

(29) Kumagai, T. Direct Observation and Control of Hydrogen-Bond Dynamics using Low-Temperature Scanning Tunneling Microscopy. *Progress in Surface Science* **2015**, *90*, 239–291.

(30) Welker, J.; Giessibl, F. J. Revealing the Angular Symmetry of Chemical Bonds by Atomic Force Microscopy. *Science* **2012**, *336*, 444–449.

(31) Wang, Y. F.; Kröger, J.; Berndt, R.; Vázquez, H.; Brandbyge, M.; Paulsson, M. Atomic-Scale Control of Electron Transport through Single Molecules. *Phys. Rev. Lett.* **2010**, *104*, 176802.

(32) Xu, J.; Zhu, X.; Tan, S.; Zhang, Y.; Li, B.; Tian, Y.; Shan, H.; Cui, X.; Zhao, A.; Dong, Z. et al. Determining Structural and Chemical Heterogeneities of Surface Species at the Single-Bond Limit. *Science* **2021**, *371*, 818–822.

(33) Schuler, B.; Fatayer, S.; Meyer, G.; Rogel, E.; Moir, M.; Zhang, Y.; Harper, M. R.; Pomerantz, A. E.; Bake, K. D.; Witt, M. et al. Heavy Oil Based Mixtures of Different Origins and Treatments Studied by Atomic Force Microscopy. *Energy Fuels* **2017**, *31*, 6856–6861.

(34) Shimizu, T. K.; Romero-Muñiz, C.; Stetsovych, O.; Carracedo-Cosme, J.; Ellner, M.; Pou, P.; Oohora, K.; Hayashi, T.; Perez, R.; Custance, O. Effect of Molecule–Substrate Interactions on the Adsorption of meso-Dibenzoporphycene Tautomers Studied by Scanning Probe Microscopy and First-Principles Calculations. *The Journal of Physical Chemistry C* **2020**, *124*, 26759–26768.

(35) Ternes, M.; González, C.; Lutz, C. P.; Hapala, P.; Giessibl, F. J.; Jelínek, P.; Heinrich, A. J. Interplay of Conductance, Force, and Structural Change in Metallic Point Contacts. *Phys. Rev. Lett.* **2011**, *106*, 016802.

(36) Ladenthin, J. N.; Frederiksen, T.; Persson, M.; Sharp, J. C.; Gawinkowski, S.; Waluk, J.; Kumagai, T. Force-Induced Tautomerization in a Single Molecule. *Nat. Chem.* **2016**, *8*, 935 – 940.

(37) Liebig, A.; Giessibl, F. J. In-Situ Characterization of O-Terminated Cu Tips for High-Resolution Atomic Force Microscopy. *Appl. Phys. Lett.* **2019**, *114*, 143103.

(38) Giessibl, F. J. A Direct Method to Calculate Tip–Sample Forces from Frequency Shifts in Frequency-Modulation Atomic Force Microscopy. *Appl. Phys. Lett.* **2001**, *78*, 123–125.

(39) Sader, J. E.; Jarvis, S. P. Accurate Formulas for Interaction Force and Energy in Frequency Modulation Force Spectroscopy. *Appl. Phys. Lett.* **2004**, *84*, 1801–1803.

(40) Bai, Y.; Buchner, F.; Wendahl, M. T.; Kellner, I.; Bayer, A.; Steinrück, H.-P.; Marbach, H.; Gottfried, J. M. Direct Metalation of a Phthalocyanine Monolayer on Ag(111) with Coadsorbed Iron Atoms. *The Journal of Physical Chemistry C* **2008**, *112*, 6087–6092.

(41) Song, C.-L.; Wang, Y.-L.; Ning, Y.-X.; Jia, J.-F.; Chen, X.; Sun, B.; Zhang, P.; Xue, Q.-K.; Ma, X. Tailoring Phthalocyanine Metalation Reaction by Quantum Size Effect. *Journal of the American Chemical Society* **2010**, *132*, 1456–1457.

(42) Smykalla, L.; Shukrynau, P.; Zahn, D. R. T.; Hietschold, M. Self-Metalation of Phthalocyanine Molecules with Silver Surface Atoms by Adsorption on Ag(110). *The Journal of Physical Chemistry C* **2015**, *119*, 17228–17234.

(43) Bao, D.-L.; Zhang, Y.-Y.; Du, S.; Pantelides, S. T.; Gao, H.-J. Barrierless On-Surface Metal Incorporation in Phthalocyanine-Based Molecules. *The Journal of Physical Chemistry C* **2018**, *122*, 6678–6683.

(44) Altenburg, S. J.; Kröger, J.; Wang, B.; Bocquet, M.-L.; Lorente, N.; Berndt, R. Graphene on Ru(0001): Contact Formation and Chemical Reactivity on the Atomic Scale. *Phys. Rev. Lett.* **2010**, *105*, 236101.

(45) Schuler, B.; Liu, W.; Tkatchenko, A.; Moll, N.; Meyer, G.; Mistry, A.; Fox, D.; Gross, L. Adsorption Geometry Determination of Single Molecules by Atomic Force Microscopy. *Phys. Rev. Lett.* **2013**, *111*, 106103.

(46) Limot, L.; Kröger, J.; Berndt, R.; Garcia-Lekue, A.; Hofer, W. A. Atom Transfer and Single-Adatom Contacts. *Phys. Rev. Lett.* **2005**, *94*, 126102.

(47) Kröger, J.; Jensen, H.; Berndt, R. Conductance of Tip–Surface and Tip–Atom Junctions on Au(111) Explored by a Scanning Tunnelling Microscope. *New J. Phys.* **2007**, *9*, 153.

(48) Kröger, J.; Néel, N.; Sperl, A.; Wang, Y. F.; Berndt, R. Single-Atom Contacts with a Scanning Tunnelling Microscope. *New J. Phys.* **2009**, *11*, 125006.

(49) Kröger, J.; Néel, N.; Limot, L. Contact to Single Atoms and Molecules with the Tip of a Scanning Tunnelling Microscope. *J. Phys.: Condens. Matter* **2008**, *20*, 223001.

(50) Berndt, R.; Kröger, J.; Néel, N.; Schull, G. Controlled Single Atom and Single Molecule Contacts. *Phys. Chem. Chem. Phys.* **2010**, *12*, 1022–1032.

(51) Bartels, L.; Meyer, G.; Rieder, K.-H. Controlled Vertical Manipulation of Single CO Molecules with the Scanning Tunneling Microscope: A Route to Chemical Contrast. *Applied Physics Letters* **1997**, *71*, 213–215.

(52) Horcas, I.; Fernández, R.; Gómez-Rodríguez, J. M.; Colchero, J.; Gómez-Herrero, J.; Baro, A. M. WSXM: A Software for Scanning Probe Microscopy and a Tool for Nanotechnology. *Rev. Sci. Instrum.* **2007**, *78*, 013705.

(53) Blöchl, P. E. Projector Augmented-Wave Method. *Phys. Rev. B* **1994**, *50*, 17953–17979.

(54) Perdew, J. P.; Burke, K.; Ernzerhof, M. Generalized Gradient Approximation Made Simple. *Phys. Rev. Lett.* **1996**, *77*, 3865–3868.

(55) Kresse, G.; Furthmüller, J. Efficient Iterative Schemes for Ab Initio Total-Energy Calculations Using a Plane-Wave Basis Set. *Phys. Rev. B* **1996**, *54*, 11169–11186.

(56) Grimme, S.; Antony, J.; Ehrlich, S.; Krieg, H. A Consistent and Accurate Ab Initio Parametrization of Density Functional Dispersion Correction (DFT-D) for the 94 Elements H-Pu. *J. Chem. Phys.* **2010**, *132*, 154104.